Available online at www.sciencedirect.com
ScienceDirect
Journal of Sound and Vibration 322 (2009) 39–59
JOURNAL OF SOUND AND VIBRATION
www.elsevier.com/locate/jsvi

Time-delayed absorber for controlling friction-driven vibration

S. Chatterjee*, P. Mahata

Department of Mechanical Engineering, Bengal Engineering and Science University, Shibpur, Howrah 711 103, West Bengal, India

Received 3 July 2008; received in revised form 22 September 2008; accepted 9 November 2008
Handling Editor: J. Lam
Available online 8 January 2009

Abstract

The efficacy of an active absorber based on the time-delayed displacement difference feedback in controlling friction-driven vibrations is discussed. Mainly two types of absorbers are considered: the tuned absorber having the natural frequency same as that of the primary system and the high-frequency absorber with the natural frequency higher than that of the primary system. The local stability analysis clearly demonstrates that the static equilibrium can be locally stabilized by appropriately selecting the control gain and the time-delay. The regions of stability are delineated in the plane of the control parameters. The robustness analysis is performed to help select the control parameters for the best performance. A method of optimizing the robustness of the system is presented. The influences of the absorber parameters on the degree of stability and the robustness are discussed. Numerical simulations of the system demonstrate that proper choices of the control parameters can also attain the global stability of the system. Numerical simulations reveal that apart from the globally stable static equilibrium or the coexisting locally stable static equilibrium with the stationary limit cycle vibrations, unbounded motions are also possible for some parameter values. Thus, care should be exercised in selecting the absorber parameters.

1. Introduction

Friction-induced self-excited vibration is a common phenomenon in mechanical and electromechanical systems. In most systems, friction-induced vibrations are highly undesirable. For example, self-excited vibration in mechanical brakes causes noise related discomfort. Another example is the controlled positioning systems that have now become an integral part of a large number of industrial production systems as well as consumer electronics product. Friction often causes high level of positioning inaccuracies by inducing self-excited oscillations around the desired position. Thus, it is not surprising that researchers have put serious efforts towards understanding the phenomena and finding suitable means of controlling such unwanted oscillations.

Researchers have identified three major mechanisms of friction-driven oscillations. The most common reason of friction-induced instability is attributed to the velocity-weakening characteristics of friction force, which is also known as the Stribeck effect. Other widely studied mechanisms are mode-coupling and sprag-slip instabilities. Elaborate and seminal reviews of the pervious research on this topic are found in [1,2].

*Corresponding author.
E-mail address: shy@mech.becs.ac.in (S. Chatterjee).

0022-460X/$ - see front matter
doi:10.1016/j.jsv.2008.11.016

Literature on controlling friction-induced vibrations is vast. Various active and passive methods of controlling friction-induced oscillations have been proposed in the literature [3–9]. Various methods including dynamic vibration absorbers, linear and nonlinear control of the tangential and the normal forces and high-frequency excitations etc. are discussed. In recent times, many researchers have investigated active control of vibrations using time-delayed state (full or partial) feedback [10–13]. Atay [14,15], Maccari [16–18] and Li et. al. [19] discuss the use of time-delayed state feedback method in controlling free, forced and parametric vibrations of the Van der Pol oscillator. Studies on the use of time-delayed feedback in controlling friction-induced instabilities and oscillations are rather limited. Elmer [20] proposes a method of controlling friction-induced oscillations by normal load modulation based on the time-delayed state feedback. His method is very similar to that proposed by Pyragas [21]. Das and Mallik [22] consider the time-delayed PD feedback control of the forced vibration of a friction-driven system. Here, control force acts in the slipping direction. Refs. [20,22] consider only the Stribeck type instability. Chatterjee [23] has discussed the time-delayed feedback control of different types of friction-induced instabilities, namely (1) Stribeck instability governed by velocity-weakening characteristics of friction force, (2) mode-coupling instability, and (3) sprag-slip instability.

In the present paper, the efficacy of a time-delayed absorber for controlling the self-excited vibration of mechanical oscillator driven by the velocity-weakening friction force is studied. A spring supported mass on a moving belt presents an archetypal model of the self-excited vibration under the velocity weakening friction force. In practice, an inertial frame of reference is not always available for fixing the control actuator. Under these circumstances, it is more convenient to attach the actuator in the form of an absorber to the primary vibrating mass. Keeping this convenience in view, a spring supported absorber mass is attached to the primary mass and an actuator is placed between the primary and the absorber mass. The time-delayed difference of the displacement of the primary mass (similar to that proposed by Elmer [20], and Pyragas [21]) is utilized to synthesize the control signal. This specific form of the controller can be very effective in stabilizing non-trivial equilibrium present in the system under consideration and most importantly the control signal goes to zero once the equilibrium is stabilized. This is not possible for an ordinary/time-delayed PD/PID feedback control. A proof-mass actuator can physically realize such an absorber. In this context, it may be mentioned that Olgac and co-workers [12] have developed an active absorber—the delayed resonator that uses time-delayed feedback for controlling forced vibrations. A mathematical model of the controlled system is developed and then the local stability of the equilibrium of the system is studied. Direct numerical simulations of the mathematical model of the system substantiate the theoretical results.

2. Mathematical model

A physical model of the controlled system is depicted in Fig. 1. The primary system is modeled as a single degree-of-freedom spring–mass system with the primary mass m_1 suspended by a spring of stiffness K_1 from a fixed support and placed upon a belt that is moving with a constant velocity $V_b(>0)$. An absorber mass (m_2) is attached with the primary mass by a spring of stiffness K_2. An actuator placed in-between the primary mass

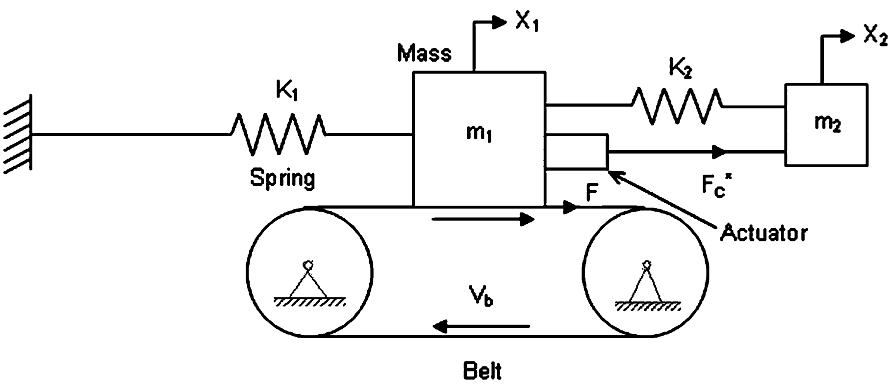

Fig. 1. Mathematical model of the system.

and the absorber mass supplies the control force (F_c). The control signal synthesized from the time-delayed state of the system actuates the actuator. The primary mass is subject to the friction force (F) generated at the belt-mass contact interface. X_1 and X_2 denote the displacements of the primary mass and the absorber mass, respectively, at any instant of time measured from an inertial frame of reference (here, fixed).

Equation of motion of the resulting two degrees-of-freedom system reads as

$$\begin{bmatrix} m_1 & 0 \\ 0 & m_2 \end{bmatrix}\begin{Bmatrix} \ddot{X}_1 \\ \ddot{X}_2 \end{Bmatrix} + \begin{bmatrix} K_1+K_2 & -K_2 \\ -K_2 & K_2 \end{bmatrix}\begin{Bmatrix} X_1 \\ X_2 \end{Bmatrix} = \begin{Bmatrix} F(V_b-\dot{X}_1) \\ 0 \end{Bmatrix} + \begin{Bmatrix} F_c \\ -F_c \end{Bmatrix}, \tag{1}$$

where the 'overdot' denotes differentiation with respect to time t.

The control force F_c is proportional to the time-delayed difference of the displacement of the primary mass as

$$F_c = K_c\{X_1(t) - X_1(t-T^*)\}, \tag{2}$$

where K_c is the control gain and T^* is the time-delay.

The friction force (F) between the primary mass and the belt is considered to follow a velocity-weakening characteristic best illustrated in Fig. 2. Various functional forms have been proposed in the literature for mathematically expressing this typical velocity dependence of the friction force. The polynomial representation with up to third order term is mathematically more amenable and widely used in the literature. However in the present paper, an exponential model of the velocity-weakening friction characteristic as proposed by Hinrichs et al. [24] is used. The exponential model, in comparison to the polynomial model, goes a long way in explaining the experimentally observed complex dynamics arising in many friction-driven systems [25]. The exponential model of the friction force used here is expressed as

$$F(v) = c^*v + N_0(\mu + \Delta\mu e^{-a^*|v|})\tanh(\beta^* v), \tag{3}$$

where v is the relative sliding velocity and c^* is the viscous component of the friction force. μ is the minimum kinetic friction coefficient and $\Delta\mu$ is the difference between the static friction coefficient and the minimum kinetic friction coefficient. N_0 is the normal load and a^* is a model parameter that determines the slope of the friction–velocity curve in the low velocity range. $\tanh(\beta^* v)$ is the continuous functional representation of signum function with $\beta^* \gg 1$.

Eqs. (1)–(3) can be recast in the following non-dimensional form:

$$\begin{bmatrix} 1 & 0 \\ 0 & 1 \end{bmatrix}\begin{Bmatrix} \ddot{y}_1 \\ \ddot{y}_2 \end{Bmatrix} + \begin{bmatrix} 1+r_m\omega_a^2 & -r_m\omega_a^2 \\ -\omega_a^2 & \omega_a^2 \end{bmatrix}\begin{Bmatrix} y_1 \\ y_2 \end{Bmatrix} = \begin{Bmatrix} f(v_0-\dot{y}_1) \\ 0 \end{Bmatrix} + \begin{Bmatrix} f_c \\ -\dfrac{1}{r_m}f_c \end{Bmatrix}, \tag{4}$$

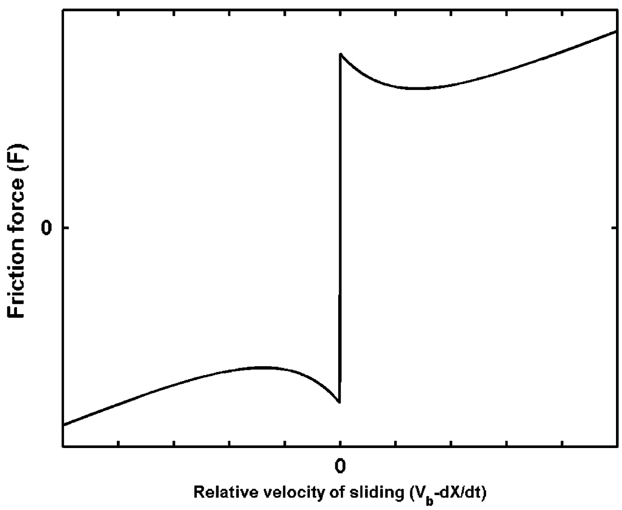

Fig. 2. Typical velocity-weakening friction characteristic.

The non-dimensional quantities are defined as

$$y_{1,2} = \frac{X_{1,2}}{x_0}, \quad v_0 = \frac{V_b}{\omega_n x_0}, \quad r_m = \frac{m_2}{m_1}, \quad \omega_a = \frac{\sqrt{\frac{K_2}{m_2}}}{\omega_n},$$

where

$$x_0 = \frac{N_0}{m_1 \omega_n^2}, \quad \omega_n = \sqrt{\frac{K_1}{m_1}}.$$

The 'overdot' denotes differentiation with respect to the non-dimensional time $\tau = \omega_n t$.

Note that v_0 is the non-dimensional belt velocity, r_m is the ratio of the absorber mass to the primary mass, and ω_a is the non-dimensional natural frequency of the absorber normalized with respect to the natural frequency ω_n of the primary system.

The non-dimensional control force f_c is expressed as

$$f_c(\tau) = k_c\{y_1(\tau) - y_1(\tau - T)\}, \tag{5}$$

where $k_c = K_c/m_1\omega_n^2$ is the non-dimensional control gain and $T = \omega_n T^*$ is the non-dimensional time-delay.

The non-dimensional form of the friction force f is given by

$$f(v_0 - \dot{y}_1) = c(v_0 - \dot{y}_1) + (\mu + \Delta\mu e^{-a|v_0 - \dot{y}_1|}) \tanh\{\beta(v_0 - \dot{y}_1)\}, \tag{6}$$

where the non-dimensional friction model parameters are defined as

$$c = \frac{c^*}{m_1 \omega_n}, \quad a = a^* \omega_n x_0, \quad \beta = \beta^* \omega_n x_0.$$

3. Local stability of the static equilibrium

3.1. Linearization around the equilibrium

In this section, the local stability of the equilibrium of the system is analyzed. Towards this end, a linearized model of the system around the equilibrium is obtained based on the assumption that the system is vibrating near the equilibrium position with the primary mass slipping on the belt. This is possible in case the magnitude of the velocity of the primary mass is always less than the belt velocity, i.e. $\dot{y}_1 < v_0$. Thus, the possibility of the reversal of the direction of the relative velocity of sliding and hence the condition of the stick-slip vibration are precluded.

The equilibrium positions y_{1e} and y_{2e} of the primary and the absorber mass are obtained as (note that as β is large and v_0 is positive, $\tanh(\beta v_0)$ is unity)

$$y_{1e} = y_{2e} = \mu + \Delta\mu e^{-a v_0} + c v_0. \tag{7}$$

By using the coordinate transformations: $z_1 = y_1 - y_{1e}$ and $z_2 = y_2 - y_{2e}$ Eq. (4) is recast as

$$\begin{bmatrix} 1 & 0 \\ 0 & 1 \end{bmatrix} \begin{Bmatrix} \ddot{z}_1 \\ \ddot{z}_2 \end{Bmatrix} + \begin{bmatrix} 1 + r_m\omega_a^2 & -r_m\omega_a^2 \\ -\omega_a^2 & \omega_a^2 \end{bmatrix} \begin{Bmatrix} z_1 \\ z_2 \end{Bmatrix} = \begin{Bmatrix} \gamma(e^{a\dot{z}_1} - 1) - c\dot{z}_1 \\ 0 \end{Bmatrix} + \begin{Bmatrix} k_c(z_1 - z_1(\tau - T)) \\ -\dfrac{1}{r_m} k_c(z_1 - z_1(\tau - T)) \end{Bmatrix}, \tag{8}$$

where $\gamma = \Delta\mu e^{-a v_0}$.

Note that the equilibrium of the system given by Eq. (8) is at the origin of the phase–space.

Expanding the nonlinear term (the first term in the RHS of Eq. (8)) of Eq. (8) in the Taylor series and neglecting the higher order terms, one finally obtains the following linearized equation of motion:

$$\begin{bmatrix} 1 & 0 \\ 0 & 1 \end{bmatrix} \begin{Bmatrix} \ddot{z}_1 \\ \ddot{z}_2 \end{Bmatrix} - \begin{bmatrix} c_e & 0 \\ 0 & 0 \end{bmatrix} \begin{Bmatrix} \dot{z}_1 \\ \dot{z}_2 \end{Bmatrix} + \begin{bmatrix} 1 + r_m\omega_a^2 & -r_m\omega_a^2 \\ -\omega_a^2 & \omega_a^2 \end{bmatrix} \begin{Bmatrix} z_1 \\ z_2 \end{Bmatrix} = \begin{Bmatrix} k_c(z_1 - z_1(\tau - T)) \\ -\dfrac{1}{r_m} k_c(z_1 - z_1(\tau - T)) \end{Bmatrix}. \tag{9}$$

Evidently, the near-equilibrium friction force generates an effective negative damping quantified as $c_e = \gamma a - c$ in Eq. (9). The self-excited oscillation of the uncontrolled system ($k_c = 0$) is possible only when c_e

assumes positive value leading to the Hopf instability of the equilibrium. It is interesting to note that the uncontrolled system has two pairs of eigenvalues with positive real parts for any positive value of c_e. It is noteworthy that the static equilibrium of the uncontrolled system is stable for any negative value of c_e. The condition $c_e = 0$ implies the marginal stability of the equilibrium of the uncontrolled system.

3.2. Stability analysis

The Laplace transform of Eq. (9) yields the following characteristic equation:

$$P(s) + Q(s)e^{-sT} = 0, \tag{10}$$

where s is a complex variable,

$$P(s) = s^4 - c_e s^3 + ks^2 - \omega_a^2 c_e s + \omega_a^2,$$

and $Q(s) = k_c s^2$, with $k = 1 - k_c + \omega_a^2(1 + r_m)$.

The roots of the characteristic Eq. (10), determine the local stability of the equilibrium. Even though Eq. (10) has infinitely many roots due to its transcendental nature, only the sign of the maximum value of the real part amongst all these roots ascertains the stability of the equilibrium. If the maximum real part is negative, the equilibrium of the original nonlinear system (Eq. (8)) is locally asymptotically stable. It is mentioned elsewhere that the uncontrolled system has two pairs of complex eigenvalues with positive real parts. On a switching boundary, one pair of roots becomes purely imaginary before migrating from the RHS s-plane to the LHS s-plane or the vice-versa. Thus substituting $s = j\omega$ into Eq. (10) and separating the real and imaginary parts, one obtains the following two equations:

$$k_c\omega^2 \cos \omega T = \omega^4 - k\omega^2 + \omega_a^2 \tag{11}$$

and

$$k_c\omega^2 \sin \omega T = -c_e\omega^3 + \omega_a^2 c_e\omega. \tag{12}$$

Squaring and adding Eqs. (11) and (12), yields the following polynomial equation in ω:

$$\omega^8 + \alpha_1\omega^6 + \alpha_2\omega^4 + \alpha_3\omega^2 + \omega_a^2 = 0, \tag{13}$$

where

$$\begin{aligned}
\alpha_1 &= c_e^2 - 2k,\\
\alpha_2 &= 2\omega_a^2 + k^2 - 2\omega_a^2 c_e^2 - k_c^2,\\
\alpha_3 &= \omega_a^4 c_e^2 - 2k\omega_a^2.
\end{aligned}$$

Positive (or trivial) real roots (ω_c) of Eq. (13) define the switching boundary. The corresponding critical values of the time-delay T_c are obtained by dividing Eq. (12) by Eq. (11) as

$$T_c = \frac{1}{\omega_c}\left[\tan^{-1}\left(\frac{-c_e\omega_c^3 + \omega_a^2 c_e\omega_c}{\omega_c^4 - k\omega_c^2 + \omega_a^2}\right) + 2i\pi\right] \quad \forall i = 0, 1, 2 \ldots \infty. \tag{14}$$

The velocity with which a pair of complex conjugate eigenvalues crosses the stability boundary at (ω_c, T_c) is computed as

$$V(\omega_c, T_c) = Re\left[\left.\frac{\mathrm{d}s}{\mathrm{d}T}\right|_{j\omega_c, T_c}\right], \tag{15}$$

where $\mathrm{d}s/\mathrm{d}T = (k_c s^3 e^{-sT})/(4s^3 - 3c_e s^2 + 2ks - \omega_a^2 c_e) - (k_c s^2 T - 2k_c s)e^{-sT})$.

The sign of the velocity of crossing V (ω_c, T_c) is defined as R (ω_c, T_c). The quantity R (ω_c, T_c) implies whether the crossing is taking place from the RHS s-plane to the LHS s-plane or the vice-versa. $R<0$ implies the crossing of a pair of complex conjugate eigenvalues from the RHS to the LHS of the s-plane. In a stable region, the total number of roots with positive real parts must be zero.

Using Eqs. (13)–(15), the local stability boundaries can be computed for any value of c_e. However, the switching boundaries and hence the stability boundary can be easily obtained for $c_e = 0$. Substituting $c_e = 0$ into Eq. (12), yields

$$\omega = \frac{n\pi}{T}, \quad n = 1, 2 \ldots\ldots \infty, \tag{16}$$

Substituting (16) into Eq. (11), one obtains the switching boundaries in the k_c–T plane as

$$\omega_a^2 T^4 - \{k + (-1)^n k_c\} n^2 \pi^2 T^2 + n^4 \pi^4 = 0, \quad n = 1, 2 \ldots\ldots \infty \tag{17}$$

Clearly, $k_c = 0$ is also a switching boundary.

The first important step before carrying out the stability analysis is to design the absorber, i.e., to select the absorber frequency ω_a and the mass ratio r_m. It is well known that the absorber frequency should be tuned to the frequency of vibration for effectively controlling forced resonant vibrations using dynamic vibration absorbers. However, no such strong theory exists in case of self-excited vibrations. The absorber frequency used in [4,8] is slightly less than the frequency of self-excitation that is also almost equal to the natural frequency of the primary system. In the present paper, the absorber frequency is chosen in the following two ranges:

1. Near the natural frequency of the primary system (here unity): Tuned absorber.
2. Near $\omega_a^2 = 10$: High-frequency absorber.

It is established in [4,8] that a higher mass ratio yields better performance. However, a high mass ratio is often not practically feasible. In the present paper, values of the mass ratio are selected less than unity. In what follows, characteristics of the local stability of the equilibrium for the tuned and the high-frequency absorbers are separately discussed.

3.2.1. Stability with tuned absorber

The region of stability in the plane of control gain vs. time-delay can be obtained from Eqs. (13)–(15) for different positive values of c_e. However, an a priori knowledge regarding the locations of the stability regions in the plane of the controlled parameters for $c_e = 0$ (the marginally stable uncontrolled system) renders the numerical computations more efficient. Fortunately, Eq. (17) is helpful in quickly identifying the stability zones for $c_e = 0$. The stability boundaries for $c_e = 0$ are delineated in Fig. 3 for different values of r_m. From Fig. 3 it is observed that there are two distinct regions of stability: the first region is located near $T = \pi$ and the second region is near $T = 2\pi$. The first region grows and the second region shrinks in size, respectively, with the increasing value of the mass ratio.

The regions of stability for different positive values of c_e and r_m are delineated in Figs. 4 and 5 and compared with that obtained for $c_e = 0$. From Fig. 4 it is inferred that the region of stability shrinks in size with the increasing value of c_e and eventually disappears beyond a critical value of c_e. From Fig. 5 it is apparent that with the increasing value of the mass ratio, the region of stability around $T = 2\pi$ gradually shrinks and then disappears, whereas the region of stability around $T = \pi$ appears after a critical value of the mass ratio and subsequently grows in size.

3.2.2. Stability with high-frequency absorber

Fig. 6 clearly demonstrates that with the increasing value of the absorber frequency, the stability region gradually shifts towards the higher positive gain and the smaller time-delay region. The stable range of the control gain increases, whereas the stable range of the time-delay decreases with the increasing value of the absorber frequency. In absence of any rigorous guidelines, the absorber frequency may be selected based on practical considerations. For example, if the first mode of vibration is of interest, the absorber frequency should be so selected that the absorber does not interact with the second mode of vibration of the primary system. One should also note that a very high gain and small time-delay controller is costly, if not practically infeasible. In what follows, the stability characteristics of the static equilibrium system with the high-frequency absorber are discussed for $\omega_a^2 = 10$.

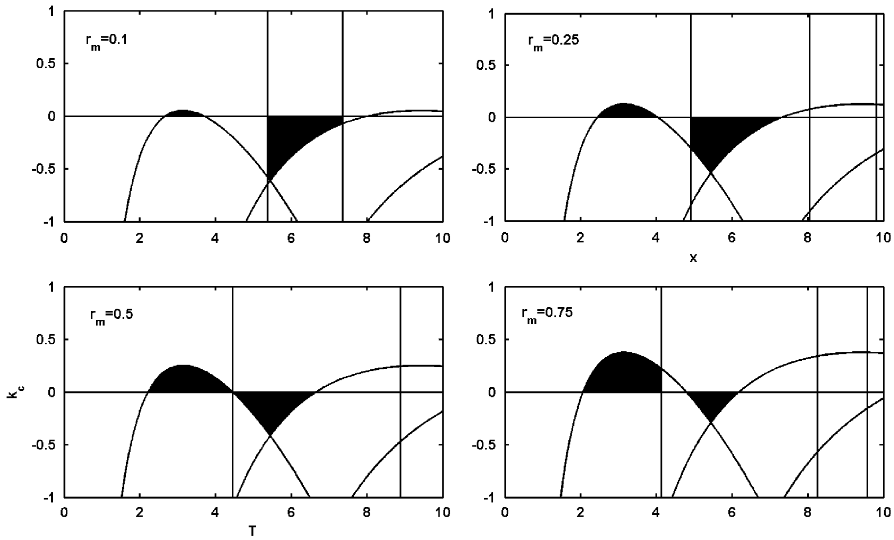

Fig. 3. Regions of stability in the plane of control parameters: $c_e = 0$ and $\omega_a = 1.0$. Black regions imply stability.

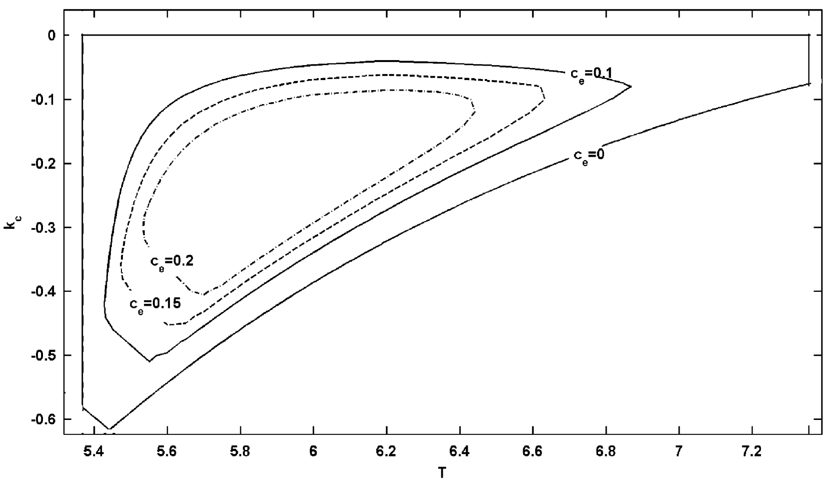

Fig. 4. Regions of stability near $T = 2\pi$: $r_m = 0.1$ and $\omega_a = 1.0$.

Fig. 7 shows the stability boundaries in the control gain vs. time-delay plane for different values of the effective damping c_e. The stability boundaries are compared with that with the marginally stable uncontrolled system corresponding to the case $c_e = 0$. Evidently, a stable region of operation exists for a wide range of the control parameters k_c and T. The lower threshold of the control gain for the stable operation increases with the increasing value of the effective damping of the primary system (c_e), whereas the upper threshold value is only marginally influence by c_e. Even though the stability of the equilibrium can be achieved for some smaller values of c_e, the proposed control strategy fails beyond a crtical value of c_e.

The effects of the mass ratio on the location of the stability region in the plane of control parameters is illustrated in Fig. 8a, which clearly demonstartes that the region of stability moves towards the zone of higher gain and smaller time-delay with the increasing value of the mass ratio. It is already evident from Fig. 6 that the effect of the increasing value of the absorber frequency is also the same. However, the high-frequency absorber with a very high mass ratio has two regions of stability: one below $T = \pi/2$ and the other below $T = \pi$, as shown in Fig. 8b.

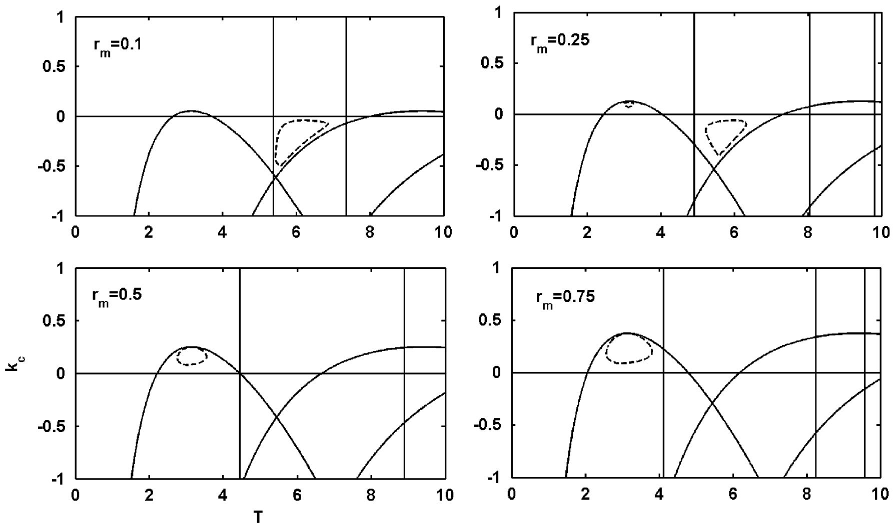

Fig. 5. Variations of the stability regions with r_m. static equilibrium is locally stable inside the dashed curves: $c_e = 0.1$.

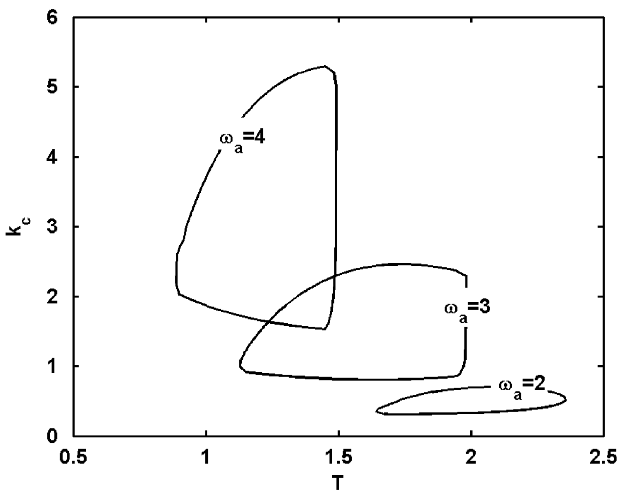

Fig. 6. Variations of the stability regions with the frequency of the absorber: $r_m = 0.1$ and $c_e = 0.1$.

4. Robustness analysis

The stability analysis presented in the previous section reveals that the exact location and the extent of the region of stability in the plane of the control parameters is sensitive to the value of the effective, negative damping parameter c_e. However in practice, an accurate estimation of the parameter c_e is never possible. Thus, it is pertinent to estimate the bound on the pertubation of the parameter c_e that the controlled system can tolerate without loosing its stability. The minimum pertubation of the parameter c_e that the system can put up with is the measure of the robustness of the control. In principle, the control and the design paramters should be appropriately selected to maximize the robustness. The basic philosophy of estimating the robustness is briefly outlined below.

A negatively damped mechanical oscillator mathematically represents the near-equilibrium dynamics of the uncontrolled system. The control force stabilizes the equilibrium by converting the overall damping of the system to a positive value. Now the stable control system is brought to the verge of instability by perturbing

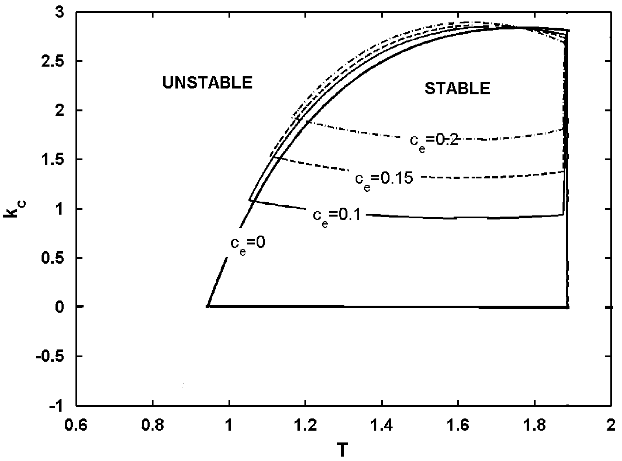

Fig. 7. Stability regions of the controlled system with the high-frequency absorber: $\omega_a^2 = 10$ and $r_m = 0.1$.

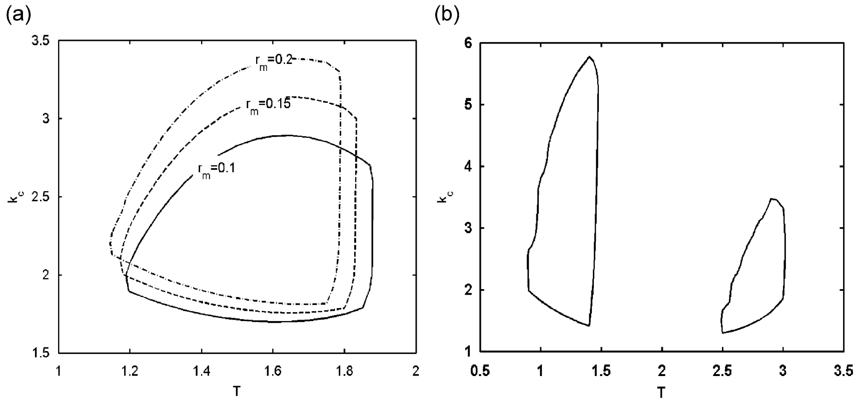

Fig. 8. Stability plots with the high-frequency absorber for different values of mass ratio: (a) $\omega_a^2 = 10$, $c_e = 0.2$ and (b) $r_m = 0.75$, $\omega_a^2 = 10$, $c_e = 0.1$.

the effective damping of the original uncontrolled system by an amount, say p. Then p is the measure of the robustness of the controlled system. In what follows, the dependence of the quantity p on the control parameters and the corresponding optimum characteristics of the same are discussed.

Let p be the perturbation of the effective damping c_e that just destabilizes the control system, which is already stabilized by the feedback. This yields the following characteristic equation:

$$P(s) + Q(s)e^{-sT} = 0, \tag{18}$$

where s is a complex variable,

$$P(s) = s^4 - (c_e + p)s^3 + ks^2 - \omega_a^2(c_e + p)s + \omega_a^2,$$

and $Q(s) = k_c s^2$, with $k = 1 - k_c + \omega_a^2(1 + r_m)$.

It may be noted that p can be of any sign: positive or negative. However, the positive value of p is of greater significance because the uncontrolled system is unstable for positive values of c_e.

Substituting $s = j\omega$ into Eq. (18) and separating the real and imaginary parts, yields

$$p = -c_e + \frac{k_c\omega^2 \sin \omega T}{\omega_a^2\omega - \omega^3} = h(\omega, T), \tag{19}$$

and

$$\cos \omega T = \frac{\omega^4 - k\omega^2 + \omega_a^2}{k_c \omega^2} = f(\omega). \tag{20}$$

Eq. (20) may have multiple real positive roots of ω that produce multiple values of p. Under these circumstances, the positive (pp) and the negative (pn) perturbation bounds on c_e can be computed according to the following pseudo code:

if min(p) > 0
    pp = min(p);
    pn = NaN;
else
    pp = max(p);
    pn = min(p);
end

4.1. Robustness with tuned absorbers

It is discussed elsewhere that the controlled system with a tuned absorber has the two regions of the stability depending upon the value of the mass ratio. Thus, the robustness analyses are performed separately for these two regions.

Case I: The stability region near $T = 2\pi$ for smaller values of r_m.

The variations of the perturbation bound (positive) with the time-delay for different values of the control gain are plotted in Fig. 9a. Similar variations for different values of the mass ratio are shown in Fig. 9b. It is

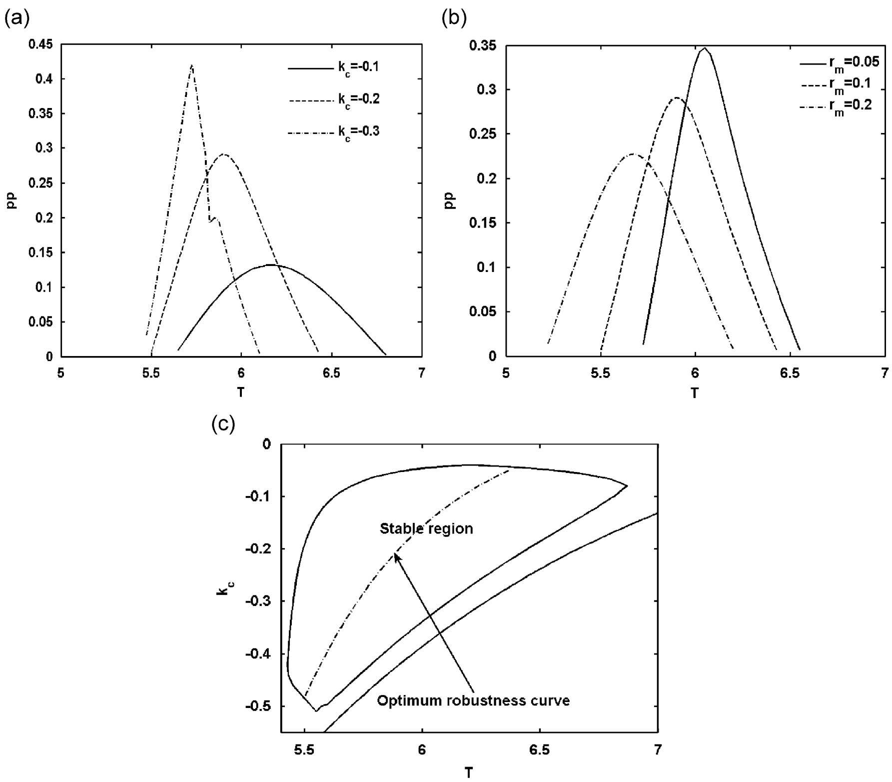

Fig. 9. Variations of positive perturbation bound with T: (a) for different gains, $c_e = 0.1$, $\omega_a = 1$, $r_m = 0.1$; (b) for different mass ratios, $c_e = 0.1$, $\omega_a = 1$, $k_c = -0.2$; and (c) optimum robustness curve, $c_e = 0.1$, $\omega_a = 1$, $r_m = 0.1$.

apparent from the above figures that with all other parameters remaining fixed, the robustness has the maximum value for a particular value of the time-delay, called the optimum time-delay. Within the particular region of stability, the maximum value of the robustness clearly increases with the increasing value of the gain and decreases with the increasing value of the mass ratio.

In order to estimate the optimum time-delay, one maximizes the quantity p with respect to the time-delay T. Towards this end, one writes

$$\frac{\mathrm{d}p}{\mathrm{d}T} = \frac{\partial h}{\partial T} + \frac{\partial h}{\partial \omega}\frac{\mathrm{d}\omega}{\mathrm{d}T} = 0. \tag{21}$$

From Eq. (20), one obtains

$$\frac{\mathrm{d}\omega}{\mathrm{d}T} = -\frac{\omega \sin \omega T}{T \sin \omega T + \dfrac{\mathrm{d}f}{\mathrm{d}\omega}}. \tag{22}$$

Substituting (22) into (21) and using (20), yields the following fifth order polynomial equation in ω^2:

$$\sum_{i=0}^{5} c_i \omega^{2i} = 0, \tag{23}$$

where $c_5 = -1$, $c_4 = 3\omega_a^2$, $c_3 = k^2 + 2\omega_a^2 - 4k\omega_a^2 - k_c^2$, $c_2 = k^2\omega_a^2 + 2\omega_a^4 - 4k\omega_a^2 - k_c^2\omega_a^2$, $c_1 = 3\omega_a^4$ and $c_0 = -\omega_a^6$.

Eq. (23) may have multiple roots. However, only the positive real roots $\omega = \omega_m$ that correspond to the positive optimum values of the time-delay $T = T_m$ qualify, where T_m is computed from Eq. (20) as

$$T_m = \frac{1}{\omega_m}\cos^{-1}\{f(\omega_m)\}, \tag{24}$$

In case of multiple qualifying roots, the optimum value is what corresponds to the maximum value of p as computed from Eq. (19).

Fig. 9c depicts the optimum robustness curve (inside the region of stability) on which the positive perturbation bound is the maximum.

Case II: The stability region near $T = \pi$ for higher values of r_m.

As mentioned earlier, this particular zone of stability exists for a tuned absorber with a higher value of the mass ratio. The variations of the perturbation bound with the time-delay within this particular zone of stability are depicted in Fig. 10a for different values of the gain. The optimum robustness curve in the gain vs. delay plane is computed as before and delineated in Fig. 10b.

4.2. Robustness with high-frequency absorbers

The stability zones for high-frequency absorbers stretch out in the positive gain and smaller delay region around $T = \pi/2$. The variations of the positive and the negative perturbation bounds with the time-delay for different values of the control gain within this specific stability boundary are plotted in Fig. 11a and b. The observations made from Fig. 11a and b are in order.

1. The positive perturbation bound increases with the increasing value of the control gain.
2. An optimum value of the time-delay exists that maximizes the positive perturbation bound on c_e.
3. The negative perturbation bound rapidly increases in magnitude with the increasing value of the time-delay.
4. The negative perturbation bound is larger in magnitude than the positive perturbation bound, particularly near the optimum value of the time-delay.

Fig. 11c depicts the optimum robustness curve corresponding to the maximum value of the positive perturbation bound on c_e.

The variations of the perturbation bounds with the control gain for different values of the mass ratio are shown in Fig. 12a and b. It is evident that with the absorber frequency fixed at the specific value, a higher

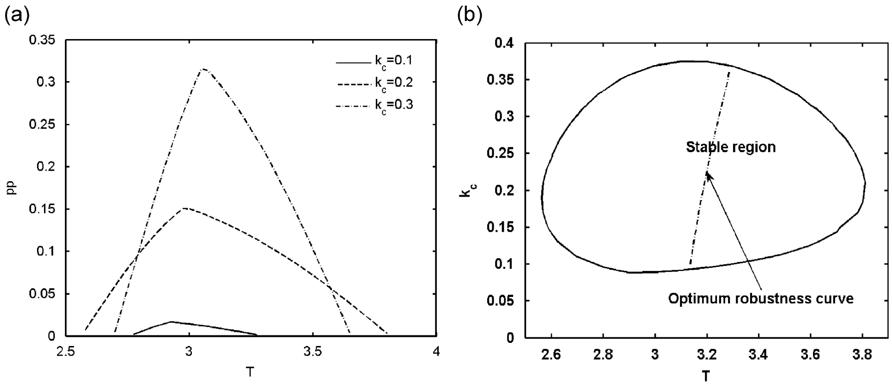

Fig. 10. (a) Variations of positive perturbation bound with T for tuned absorber for different gains, $c_e = 0.1$, $\omega_a = 1$, $r_m = 0.75$ and (b) optimum robustness curve, $c_e = 0.1$, $\omega_a = 1$, $r_m = 0.75$.

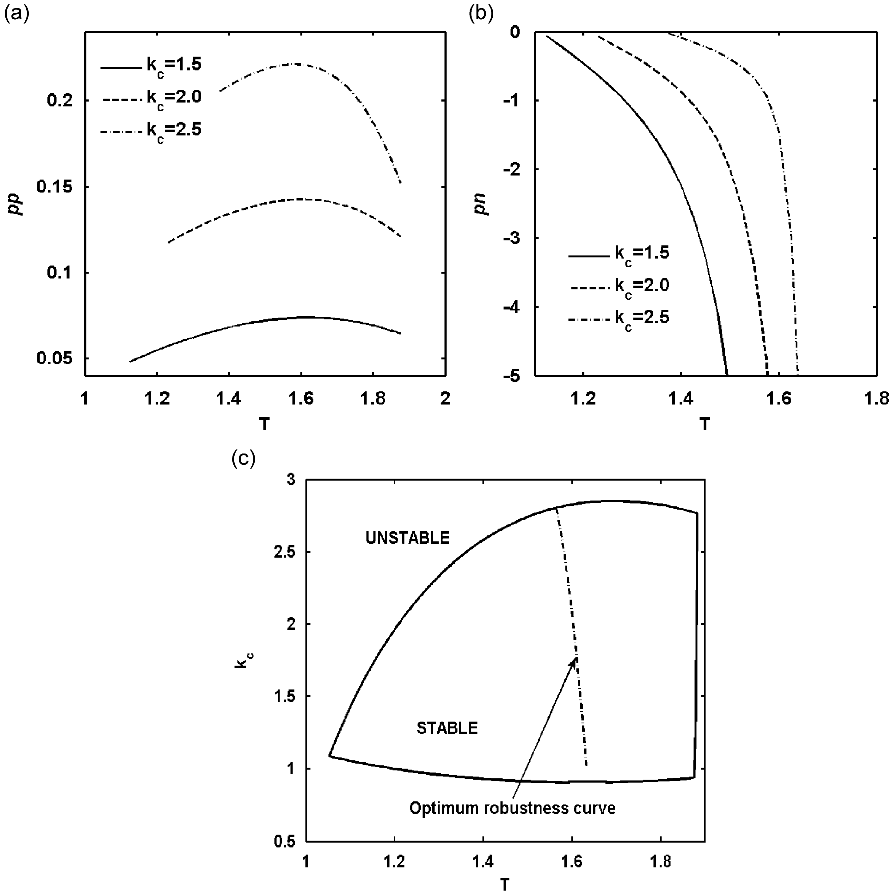

Fig. 11. (a) and (b) Variations of positive and negative perturbation bounds on c_e with the time-delay for different values of the control gain, $\omega_a^2 = 10$, $r_m = 0.1$, $c_e = 0.1$ and (c) optimum robustness curve, $\omega_a^2 = 10.0$, $r_m = 0.1$, $c_e = 0.1$.

robustness is achieved for a lower mass ratio. Fig. 12c and d show the variations of the perturbation bounds with the time-delay for different absorber frequencies. Clearly higher robustness is achieved with lower absorber frequency. However, the absorber natural frequency can be decreased only up to a limit from the nominal value because the optimum value gradually shifts towards the stability boundary. Selecting parameter

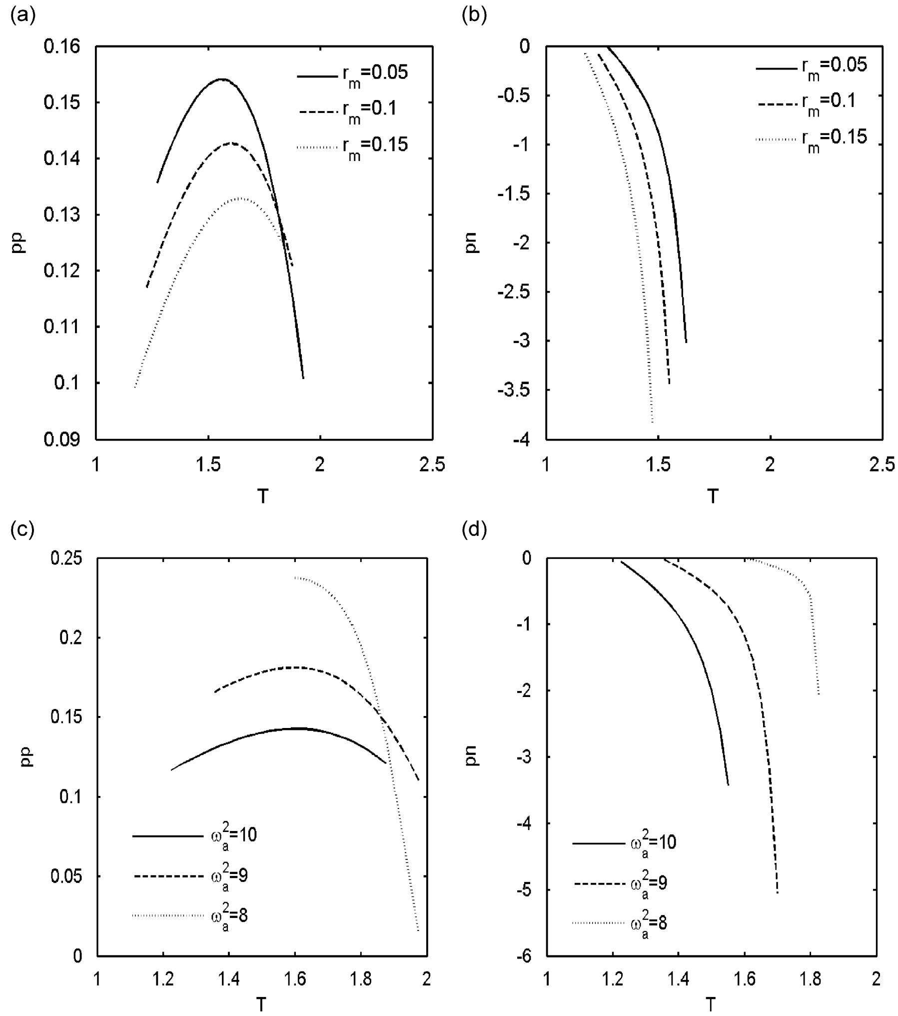

Fig. 12. Variations of the perturbation bounds with delay: (a) and (b) for different r_m, $\omega_a^2 = 10.0$, $k_c = 2$, $c_e = 0.1$; (c) and (d) for different ω_a. $k_c = 2$, $c_e = 0.1$, $r_m = 0.1$.

values on or near the stability boundary is not advisable as the system may be pushed into the unstable zone under a slight parametric perturbation. The above results clearly suggest that a relatively compliant absorber is better.

Fig. 12a–d clearly indicate that with the absorber frequency close to $\sqrt{10}$, the optimum value of the time-delay for the maximum robustness is approximately around $\pi/2$.

5. Degree of stability

The degree of stability is quantified as the minimum absolute value of the real part of the poles of a stable system. An useful approach to compute the region having a particular degree of stability or higher inside the stable region is to shift the s-plane axis by a constant positive quantity say σ, such that

$$s = s_1 - \sigma. \tag{25}$$

Substituting the above in Eq. (10), yields the following quasi-polynomial in the new variable s_1:

$$P_1(s_1) + Q_1(s_1)e^{-s_1 T} = 0, \tag{26}$$

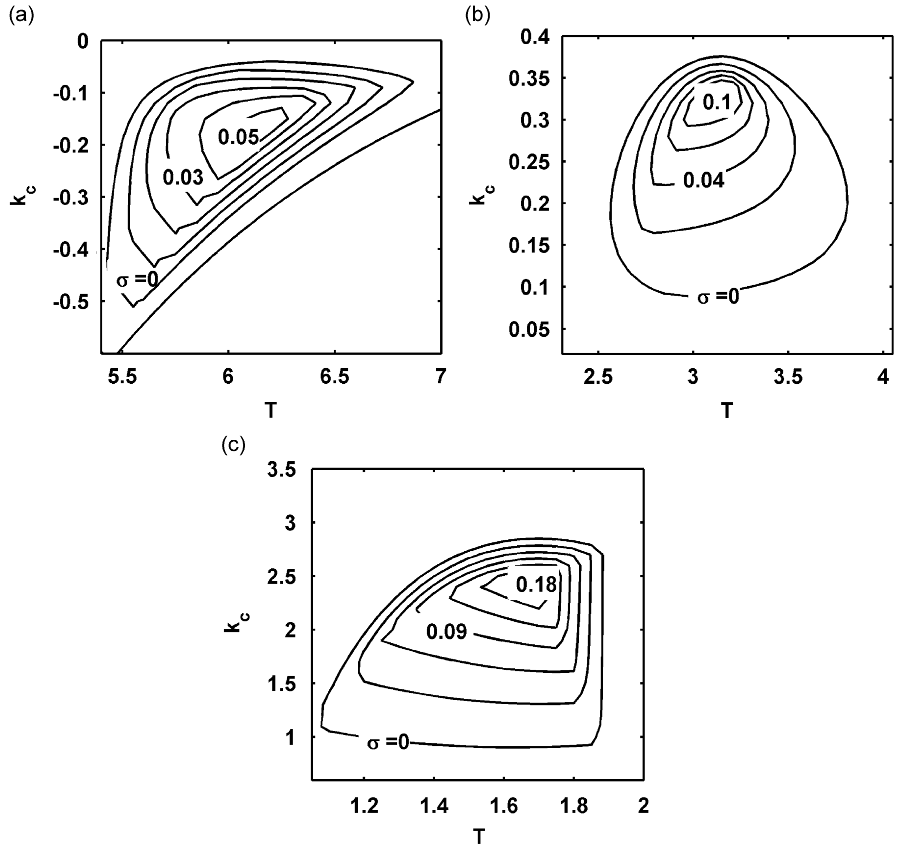

Fig. 13. Iso-σ lines: (a) for the tuned absorber, $c_e = 0.1$, $r_m = 0.1$, $\omega_a = 1$; (b) for the tuned absorber, $c_e = 0.1$, $r_m = 0.75$, $\omega_a = 1$; and (c) for the high-frequency absorber, $c_e = 0.1$, $r_m = 0.1$, $\omega_a = 10^{1/2}$.

where

$$P_1(s_1) = s_1^4 + a_3 s_1^3 + a_2 s_1^2 + a_1 s_1 + a_0,$$

with

$$a_3 = -4\sigma - c_e, \quad a_2 = 1 + 3c_e\sigma + 6\sigma^2 + \omega_a^2 + r_m\omega_a^2 - k_c,$$
$$a_1 = 2k_c\sigma - (c_e + 2\sigma + 2r_m\sigma)\omega_a^2 - 2\sigma - 3c_e\sigma^2 - 4\sigma^3,$$
$$a_0 = \omega_a^2(1 + \sigma^2 + r_m\sigma^2 + c_e\sigma) + c_e\sigma^3 + \sigma^2(1 - k_c) + \sigma^4,$$

and

$$Q_1(s_1) = e^{\sigma T}(k_c s_1^2 - 2k_c\sigma s_1 + k_c\sigma^2).$$

Now using the same procedure as described in Section 3.2, the stability boundary is obtained from Eq. (26). This stability boundary represents a contour line having the degree of stability σ, i.e. by selecting the parameters on this contour will ensure that the real part of the pole closest to the imaginary axis is $-\sigma$. The degree of stability is higher than σ for any value of the control parameters inside the σ-contour. Several such iso-σ lines can be plotted inside the stable region of operation. Iso-σ lines for the tuned and the high-frequency absorbers are shown in Fig. 13a–c. From these figures, it is evident that the high-frequency absorber produces higher degree of stability than that produced by the tuned absorber. However beyond a particular value of the absorber frequency, the maximum degree of stability again decreases with the increasing value of the absorber frequency (results are not shown). The degree of stability of the tuned absorber generally decreases with the increasing mass ratio within a lower range of values for which the stability boundary is located near $T = 2\pi$. However, the degree of stability of the tuned absorber can be significantly improved by increasing the mass ratio to a high value that changes the location of the stability boundary towards $T = \pi$. However, this is not true with the high-frequency absorber. The degree of stability generally decreases with the increasing value of the mass ratio.

6. Numerical simulations

The stability analysis discussed in Section 3 considers only the local stability of the equilibrium. Therefore for the parameter values selcted inside the stable region of operation, the equilibrium is reached only from a specific region in the phase–space (the basin of attraction of the equilibrium). This means that the locally stable equilibrium may coexist with a stable limit cycle oscillation. However, global stability is also essential for a successful control system designed for suppressing the friction-induced oscillation because only in a globally stable system, the motions, starting from any arbitrary initial condition, settle down to the equilibrium. As expected, the local stability analysis does not provide any information about the global stability of the equilibrium. In order to establish the global stabiltiy of the proposed system, direct numerial simulations of a MATLAB SIMULINK model of the system are employed. The parameter values used in the numerical simulations are: friction model parameters: $\mu = 0.2$, $\Delta\mu = 0.2$, $a = 1.0$, $c = 0.0$ and non-dimensional belt velocity $v_0 = 0.15$ (these parameter values correspond to $c_e = 0.1721$).

6.1. Numerical simulations with tuned absorber

The parameter values of the tuned absorber used for numerial simulations are $\omega_a = 1$ and $r_m = 0.1$. In order to maintain a good robustness as well as a high degree of stability, the control parameters are chosen as $k_c = 0.2$ and $T = 6.0$. The phase–plane plots of the trajectories of the controlled system starting from different initial conditions are depicted in Fig. 14. The converging trajectories to the equilibrium from different initial

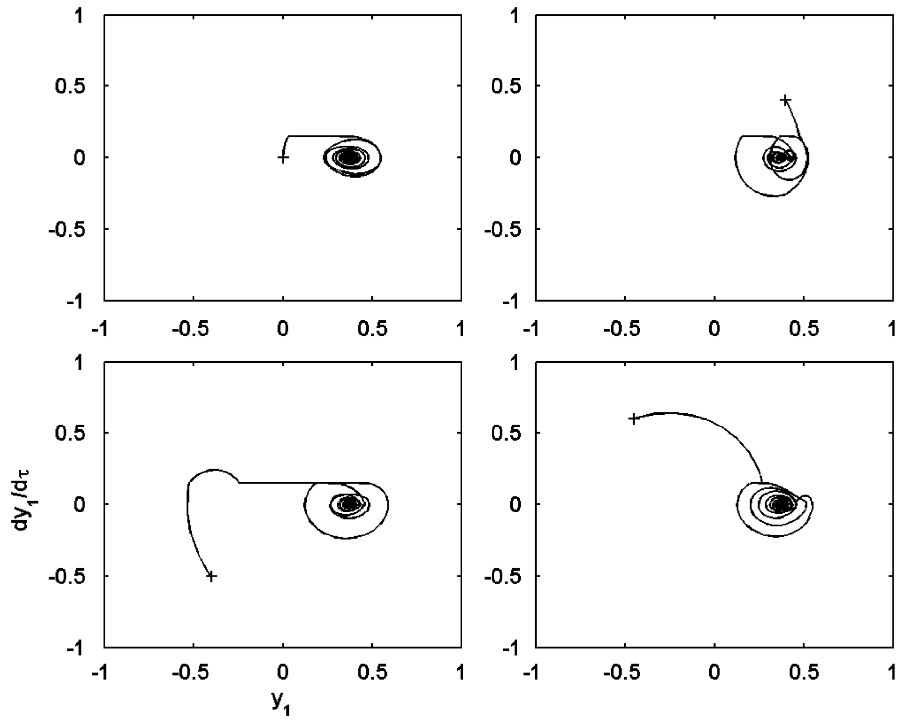

Fig. 14. Trajectories of the controlled system in the phase plane from different initial conditions: $T = 6.0$ and $k_c = -0.2$. + denotes the initial point.

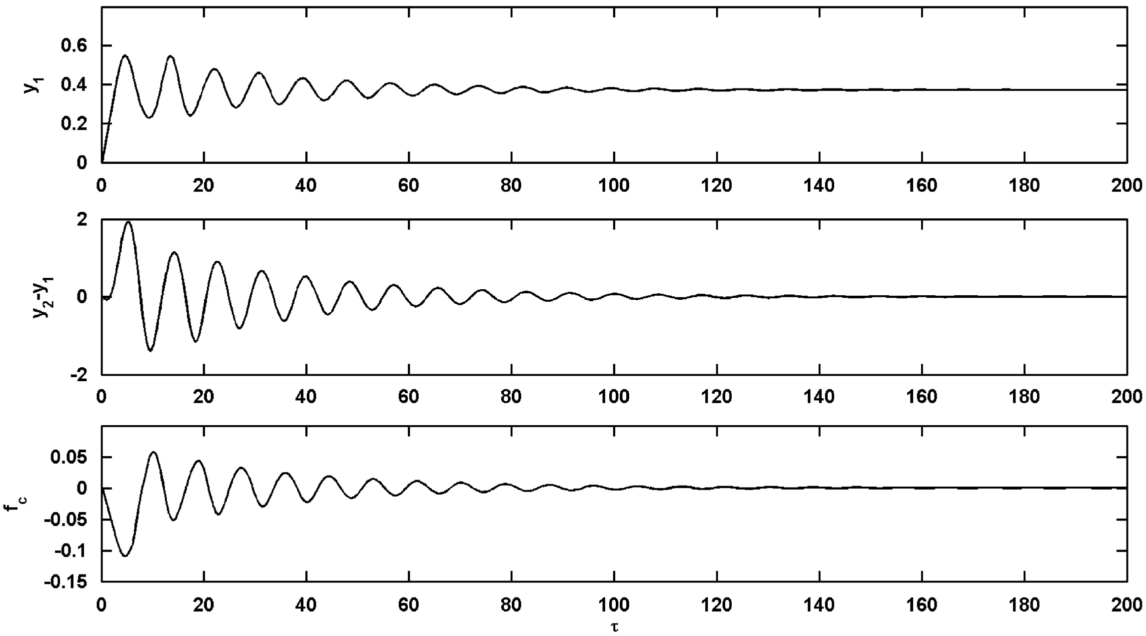

Fig. 15. Time history plots with tuned absorber: $T = 6$ and $k_c = -0.2$. These plots are generated for trivial initial conditions.

conditions clearly demonstrate the global stability of the proposed control system. The time history plots of the displacement of the primary mass, the absorber deformation, and the control force are presented in Fig. 15.

However, for the control parameters chosen very close to the stability boundary, the stable equilibrium often coexists with a limit cycle oscillation. Overall, it may be concluded that the equilibrium is globally stable for the control parameters chosen from a region around the maximum robustness curve and the contour line with a high value of σ.

The results of the numerical simulation of the system with the tuned absorber having a high mass ratio are not presented here. However, the results validate the earlier conclusions that the degree of stability of the tuned absorber improves by using a high mass ratio that relocates the stability region around $T = \pi$.

6.2. Numerical simulations with high-frequency absorber

The foregoing analysis shows that for the high-frequency absorber, the stability region is around $T = \pi/2$ and higher positive control gain. The parameter values used for the high-frequency absorber are $\omega_a = \sqrt{10}$ and $r_m = 0.1$. In order to maintain a good robustness as well as a high degree of stability, the control parameters are chosen as $k_c = 2.5$ and $T = \pi/2$. The phase–plane plots of the trajectories of the controlled system starting from different initial conditions are depicted in Fig. 16. The converging trajectories to the equilibrium from different initial conditions clearly demonstrate the global stability of the proposed control system. Time history plots of the displacement of the primary mass, the absorber deformation, and the control force are presented in Fig. 17. Comparing Figs. 15 and 17, it is apparent that the vibration staring from the same initial conditions settles faster to the equilibrium in case of the high-frequency absorber. Evidently, the maximum deformation of the high-frequency absorber is less than that of the tuned absorber. However, the maximum control force is higher in case of the high-frequency absorber.

Other than the globally stable motions as shown in Figs. 16 and 17, there exist other types of motions for the parameter values chosen at different points inside/outside the local stability region. Results of the detailed numerical simulations are available in [26]. The numerical simulations are carried out at thirteen different points in the parameter plane as shown in Fig. 18. The summary of these different types of motions observed during numerical simulations are tabulated in Table 1. From the analysis and the results of the numerical

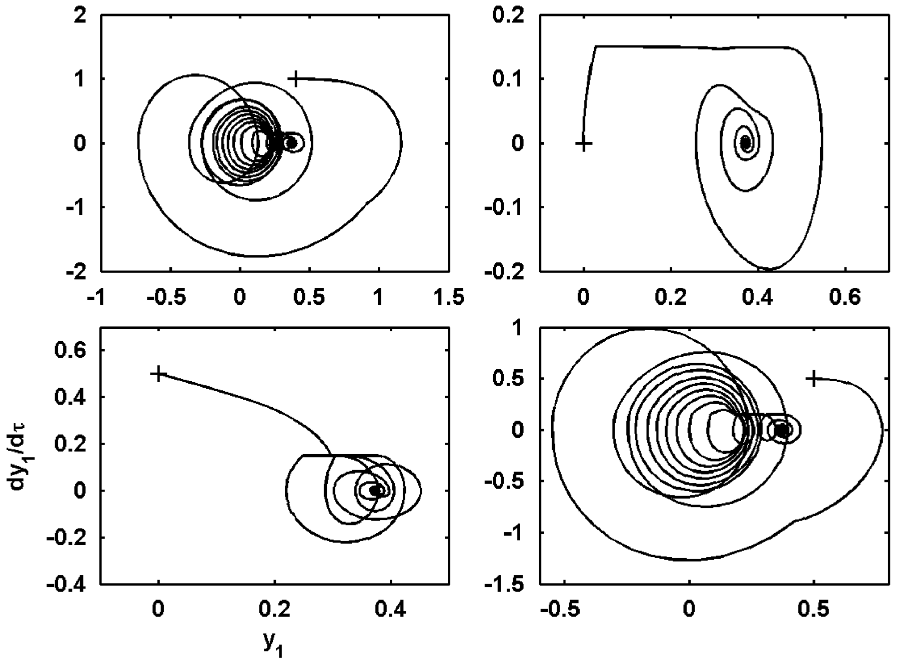

Fig. 16. Trajectories of the controlled system in the phase plane from different initial conditions: $T = \pi/2$ and $k_c = 2.5$. + denotes the initial point.

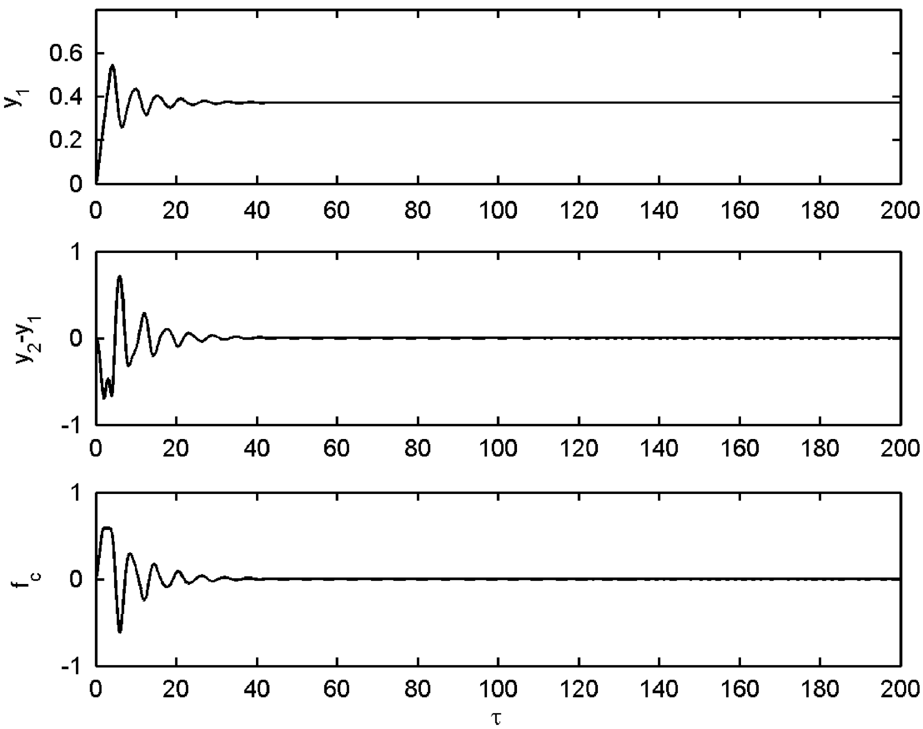

Fig. 17. Time history plots with high-frequency absorber. $T = \pi/2$ and $k_c = 2.5$. These plots are generated for trivial initial conditions.

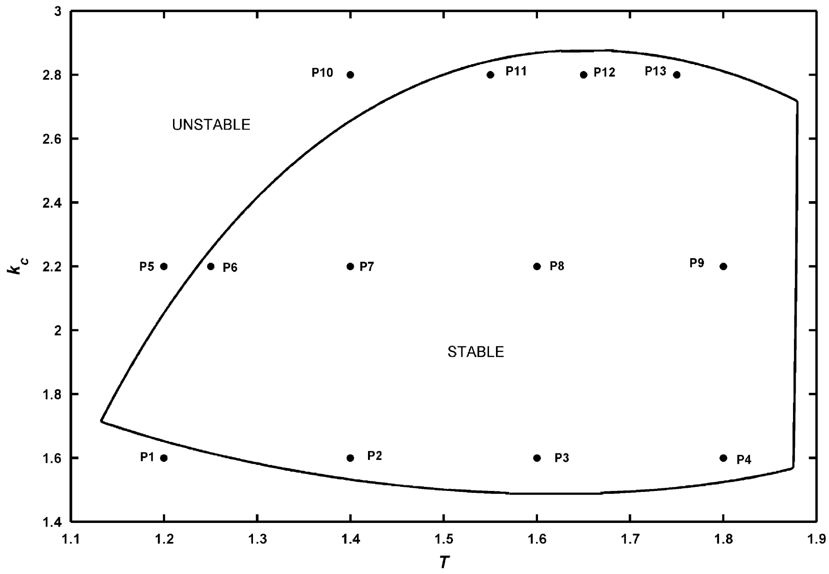

Fig. 18. Points on the stability plot where numerical simulations are carried out: $c = 0$, $\omega_a^2 = 10$, $r_m = 0.1$, $\mu = 0.2$, $\Delta\mu = 0.2$, and $a = 1$. The effective damping corresponding to the friction parameters considered is $c_e = 0.1721$.

simulations, it may be conjectured that the global stability is achieved when the control parameters are chosen deep inside the stability region and away from the boundary. The best results are obtained when the parameter values are chosen around the maximum robustness curve and the σ-contour lines with a high value of σ. However, the existence of unbounded motions near the stability boundary (towards the lower threshold of the time-delay) may create a bit of practical difficulty in implementing the high-frequency absorber, because the result may be catastrophic in case of the failure of the control. Using a bounded control input can possibly circumvent this problem. This may be addressed in a future work.

7. Conclusions

The paper presents a theoretical study on the use of time-delayed active absorber for controlling friction-induced vibration. A single degree-of-freedom mechanical oscillator vibrating on a belt moving with a constant velocity represents the primary system. The velocity-weakening characteristic of the friction force is considered to be the major source of the self-excitation. The absorber consists of a spring-mass system with one end of the spring attached to the primary mass and the other end to the absorber mass. The actuator is placed in-between the primary and the absorber mass. The time-delayed difference of the displacement of the primary mass is used as the feedback to control the actuator. A system of delay differential equations mathematically describes the two degrees-of-freedom model of the control system.

Mainly two types of absorbers, with different natural frequencies, are considered. In one type, the absorber natural frequency is the same as that of the primary system (here unity); this is termed as the tuned absorber. Another type has the natural frequency larger (here $10^{1/2}$) than the natural frequency of the primary system and this is termed as the high-frequency absorber. Stability and robustness analysis of the system with the two types of absorbers are performed. A method of optimizing the robustness of the control is proposed.

From the local stability and robustness analysis, the following important conclusions are drawn regarding the qualitative dynamic behavior of the system:

1. The tuned absorber with smaller mass ratio can stabilize the static equilibrium for smaller negative gain and the time-delay around 2π.
2. The tuned absorber with higher mass ratio stabilizes the static equilibrium for positive gain and the time-delay around π.

Table 1
Results of numerical simulations with the high-frequency absorber.

Simulation point	Dynamics with initial condition set-I	Dynamics with initial condition set-II	Remarks
P1	$y_1(0)=0.5$, $y_2(0)=0.2$, $v_1(0)=1$, $v_2(0)=2$: large amplitude vibration of the absorber mass	$y_1(0)=0$, $y_2(0)=0$, $v_1(0)=0$, $v_2(0)=0$: small amplitude vibration of the absorber mass	Equilibrium unstable
P2	$y_1(0)=0$, $y_2(0)=0$, $v_1(0)=0$, $v_2(0)=0$: converging to equilibrium	$y_1(0)=0.2$, $y_2(0)=0.8$, $v_1(0)=0$, $v_2(0)=0$: converging to equilibrium	Equilibrium globally stable; slow convergence from IC set-I
P3	$y_1(0)=0$, $y_2(0)=0$, $v_1(0)=0$, $v_2(0)=0$: converging to equilibrium	$y_1(0)=0.8$, $y_2(0)=0$, $v_1(0)=0$, $v_2(0)=0$: converging to equilibrium	Equilibrium globally stable; faster rate of convergence than the previous point from IC set-I
P4	$y_1(0)=0$, $y_2(0)=0$, $v_1(0)=0$, $v_2(0)=0$: converging to equilibrium	$y_1(0)=0.8$, $y_2(0)=0$, $v_1(0)=0$, $v_2(0)=0$: converging to equilibrium	Equilibrium globally stable; slower rate of convergence than the previous point from IC set-I
P5	$y_1(0)=0$, $y_2(0)=0$, $v_1(0)=0$, $v_2(0)=0$: unbounded solution		Equilibrium unstable
P6	$y_1(0)=0.2$, $y_2(0)=0$, $v_1(0)=0$, $v_2(0)=0$: unbounded solution	$y_1(0)=0$, $y_2(0)=0$, $v_1(0)=0$, $v_2(0)=0$: converging to equilibrium	Equilibrium is locally stable. Global motion is unbounded implying the existence of an unstable limit cycle in the phase space
P7	$y_1(0)=0.4$, $y_2(0)=0$, $v_1(0)=0$, $v_2(0)=0$: converging to a limit cycle oscillation	$y_1(0)=0$, $y_2(0)=0$, $v_1(0)=0$, $v_2(0)=0$: converging to equilibrium	Equilibrium is locally stable and surrounded by a stable limit cycle in the phase space
P8	$y_1(0)=0$, $y_2(0)=0$, $v_1(0)=0$, $v_2(0)=0$: converging to equilibrium	$y_1(0)=0.6$, $y_2(0)=0.8$, $v_1(0)=2$, $v_2(0)=1$: converging to equilibrium	Equilibrium globally stable
P9	$y_1(0)=0$,$y_2(0)=0$, $v_1(0)=0$, $v_2(0)=0$: converging to equilibrium	$y_1(0)=0.6$, $y_2(0)=0.8$, $v_1(0)=3$, $v_2(0)=1$: converging to equilibrium	Equilibrium globally stable
P10	$y_1(0)=0$, $y_2(0)=0$, $v_1(0)=0$, $v_2(0)=0$: unbounded motion		Equilibrium unstable
P11	$y_1(0)=0.4$, $y_2(0)=0$, $v_1(0)=1$, $v_2(0)=0$: unbounded motion	$y_1(0)=0$, $y_2(0)=0$, $v_1(0)=0$, $v_2(0)=0$: converging to equilibrium	Equilibrium is locally stable. Global motion is unbounded implying the existence of an unstable limit cycle in the phase space
P12	$y_1(0)=0.4$, $y_2(0)=0$, $v_1(0)=0$, $v_2(0)=0$: converging to equilibrium	$y_1(0)=0.4$, $y_2(0)=0$, $v_1(0)=0$, $v_2(0)=0$: unbounded motion	Equilibrium is locally stable. Global motion is unbounded implying the existence of an unstable limit cycle in the phase space
P13	$y_1(0)=0.2$, $y_2(0)=0$, $v_1(0)=2$, $v_2(0)=0$: converging to equilibrium	$y_1(0)=0.6$, $y_2(0)=0.8$, $v_1(0)=2$, $v_2(0)=1$: converging to equilibrium	Equilibrium globally stable

3. The high frequency absorber stabilizes the equilibrium with relatively lager positive control gain and the time-delay around $\pi/2$.
4. Tuned absorber with higher mass ratio offers higher degree of stability and robustness.
5. High-frequency absorber with smaller mass ratio gives better degree of stability and robustness.

The effects of the absorber parameters on the stability, robustness and the degree of stability clearly suggest that the higher degree of stability and robustness is possible if the region of stability is located around $T=\pi/2$ or $T=\pi$, the first location being more preferable.

Direct numerical simulations are performed for both types of absorbers with the control parameters selected near the optimum robustness curve and the contour line having high degree of stability. The trajectories are observed to settle to the static equilibrium irrespective of the initial conditions chosen. This establishes the global stability of the system with both types of absorbers. Overall, it is observed that the equilibrium is globally stable with the control parameters chosen near the maximum robustness curve as well as the contour lines of high degree of stability that are generally located far from the stability boundary. However if the control parameters are selected closer to the boundary, other types of motions including limit cycle oscillations are possible even within the local stability boundary. Detailed numerical simulations reveal that unlike the system with the tuned absorber, the system with the high frequency absorber shows a rich variety of dynamics some of which are detrimental to the system. These include high amplitude vibrations of the absorber and even unbounded motions.

Based on the analyses and numerical simulations, qualitative comparisons between the basic dynamic characteristics of the two types of absorbers can be made. The tuned absorber is functional for smaller values of the control gain and larger values of the time-delay and hence is practically more attractive. Moreover, the absence of high amplitude vibrations and unbounded motions outside the global stability region makes the situation comfortable for the designer. However, the absorber deformation is on the higher side. On the other hand, the high-frequency absorber operates on higher values of the control gain and smaller values of the time-delay. The high-frequency absorber offers relatively higher degree of stability and has lower deformation. However, the major disadvantage with the high-frequency absorber is that outside the global stability region, the amplitude of vibration may be higher than that of the uncontrolled system. In some worst cases, the system motions are unbounded leading to catastrophic failures. Moreover, a high-frequency absorber may interact with higher modes of vibration of the primary system that are not considered in the present mathematical model.

The present theoretical study clearly shows the possibility of using an active time-delayed absorber for controlling any form of self-excited vibration of an elastic structure. The particular control law considered in the present study is just one possibility out of many. Other possibilities may be time-delayed velocity and acceleration feedback etc. Future research should concentrate on exploring such other possibilities.

References

[1] R.A. Ibrahim, Friction-induced vibration, chatter, squeal, and chaos, part II: dynamics and modeling, *Transactions of ASME, Applied Mechanics Review* 47 (7) (1994) 227–253.

[2] E.J. Berger, Friction modeling for dynamic system simulation, *Transactions of ASME, Applied Mechanics Review* 55 (6) (2002) 535–577.

[3] B. Armstrong-Hélouvry, P. Dupont, C. Canudas de Wit, A survey of models, analysis tools and compensation methods for the control of machines with friction, *Automatica* 30 (7) (1994) 1083–1138.

[4] M.A. Heckl, D. Abrahams, Active control of friction driven oscillations, *Journal of Sound and Vibration* 193 (1) (1996) 417–426.

[5] K. Popp, M. Rudolph, Vibration control to avoid stick-slip motion, *Journal of Vibration and Control* 10 (2004) 1585–1600.

[6] J.J. Thomsen, Using fast vibrations to quench friction-induced oscillations, *Journal of Sound and Vibration* 228 (5) (1999) 1079–1102.

[7] S. Chatterjee, T.K. Singha, S.K. Karmakar, Effect of high-frequency excitation on a class of mechanical systems with dynamic friction, *Journal of Sound and Vibration* 269 (2004) 61–89.

[8] S. Chatterjee, Non-linear control of friction-induced self-excited vibration, *International Journal of Nonlinear Mechanics* 42 (3) (2007) 459–469.

[9] S. Chatterjee, On the design criteria of dynamic vibration absorbers for controlling friction-induced oscillations, *Journal of Vibration and Control* 14 (3) (2008) 397–415.

[10] A. Maccari, Vibration control for the primary resonance of a cantilever beam by a time delay state feedback, *Journal of Sound and Vibration* 259 (2) (2003) 241–251.

[11] R. Sipahi, N. Olgac, Active vibration suppression with time delayed feedback, *Journal of Vibration and Acoustics—Transactions of ASME* 125 (2003) 384–388.

[12] N. Olgac, B.T. Holm-Hansen, A novel active vibration absorption technique: delayed resonator, *Journal of Sound and Vibration* 176 (1994) 93–104.

[13] J.C. Ji, A.Y.T. Leung, Resonances of a non-linear s.d.o.f. system with two time-delay in linear feedback control, *Journal of Sound and Vibration* 253 (5) (2002) 985–1000.

[14] F.M. Atay, Van der Pol's oscillator under delayed feedback, *Journal of Sound and Vibration* 218 (2) (1998) 333–339.

[15] F.M. Atay, Delayed feedback control of oscillations in nonlinear planar systems, *International Journal of Control* 75 (2002) 297–304.

[16] A. Maccari, Vibration control of parametrically excited Lienard system, *International Journal of Nonlinear Mechanics* 41 (2006) 146–155.

[17] A. Maccari, Vibration control for the primary resonance of a cantilever beam by a time delay state feedback, *Journal of Sound and Vibration* 259 (2) (2003) 241–251.

[18] A. Maccari, Vibration control for the primary resonance of the van der Pol oscillator by a time delay state feedback, *International Journal of Nonlinear Mechanics* 38 (2003) 123–131.

[19] X. Li, J.C. Ji, C.H. Hansen, C. Tan, Response of a Duffing–Van der Pol oscillator under delayed feedback control, *Journal of Sound and Vibration* 291 (2006) 644–655.

[20] F.-J. Elmer, Controlling friction, *Physical Review E* 57 (1998) 4903–4906.
[21] K. Pyragas, *Physics Letters A* 170 (1992) 421–424.
[22] J. Das, A.K. Mallik, Control of friction driven oscillation by time-delayed state feedback, *Journal of Sound and Vibration* 297 (3–5) (2006) 578–594.
[23] S. Chatterjee, Time-delayed feedback control of friction-induced instability, *International Journal of Nonlinear Mechanics* 42 (2007) 1127–1143.
[24] N. Hinrichs, M. Oestreich, K. Popp, On the modeling of friction oscillators, *Journal of Sound and Vibration* 216 (3) (1998) 435–459.
[25] R. Horvath, Experimental Investigation of Excited and Self-excited Vibration, Master's Thesis, University of Technology and Economics, Budapest, 2000 ⟨http://www.auburn.edu/~horvaro/index2.htm⟩.
[26] P. Mahata, Controlling Friction-induced Self-excited Oscillation by Time-delayed Feedback, M.E. Thesis, Department of Mechanical Engineering, Bengal Engineering and Science University, Shibpur, 2008.